A Preventive Dispatching Method for High Wind Power-Integrated Electrical Systems Considering Probabilistic Transient Stability Constraints

YUCHUAN CHEN[ID]**, S. MAHDI MAZHARI**[ID] **(Member, IEEE), C. Y. CHUNG**[ID] **(Fellow, IEEE), AND SHERIF O. FARIED**[ID] **(Senior Member, IEEE)**

Department of Electrical and Computer Engineering, University of Saskatchewan, Saskatoon, SK S7N 5A9, Canada

CORRESPONDING AUTHOR: C. Y. CHUNG (c.y.chung@usask.ca)

ABSTRACT This paper proposes a probabilistic transient stability-constrained preventive dispatching method for power systems under a high inclusion of wind power. First, a set of instability mode (IM)-categorized probabilistic transient stability constraints (PTSCs) are constructed, which facilitate the development of a dispatching plan against various fault scenarios. Next, to avoid massive transient stability simulations in each dispatching operation, a machine learning-based model is trained to predict the critical clearing time (CCT) and IM for all preconceived fault scenarios. Based on the predictions, the system operation plan is assessed with respect to the PTSCs. Then, the sensitivity of the probabilistic level of the CCT is calculated to the active power generated from the critical generators for each IM category. Accordingly, the implicit PTSCs are converted into explicit dispatching constraints, and the dispatch is rescheduled to ensure the probabilistic stability requirements of the system are met at an economical operating cost. The proposed approach is validated on two modified IEEE test systems, reporting high computational efficiency and high-quality solutions.

INDEX TERMS Critical clearing time (CCT), machine learning, optimal power flow, power dispatch, probabilistic transient stability, uncertainties, wind power.

NOTATION

A. SETS AND INDICES

$\Omega^B, \Omega^G, \Omega^L$ Sets of buses, synchronous generators (SGs), and transmission lines, respectively.

Ω^{IM} Set of all instability modes (IMs) that may appear in the network.

Ω^{OP} Set of possible operating points.

Ω^w Set of possible wind power generation scenarios.

$\Omega^{L,OP}$ Set of fault scenarios to be tested in dispatching operations, which consider each fault at L for all operating points in Ω^{op}.

$\Omega^{CCT,IM}$ Set of data pairs (CCT, IM), where each pair is the CCT and IM of a fault scenario in $\Omega^{L,OP}$.

Ω_k^C, Ω_k^R Sets of critical and remaining SGs of IM k, respectively.

k Index of Ω^{IM}.

B. PARAMETERS

α_k The threshold value of CCT set for IM k.

β_k Acceptable security level set for ρ_k (CCT > α_k).

T Time interval between two consecutive dispatching operations.

$\underline{\Delta P}$ A threshold value to check the maximum power output change in all SGs between two consecutive iterations.

C. VARIABLES

ρ_k (CCT $> \alpha_k$)	Probability of CCT $> \alpha_k$.
$\boldsymbol{u}$	Control variables in the power dispatch.
$\boldsymbol{\varepsilon}$	Uncertainties that might change the system operating point.
ξ_k	Sensitivity of ρ_k (CCT $> \alpha_k$) to the active power generated from Ω_k^C.
L	A list of fault lines created by sampling the elements in Ω^L according to $\boldsymbol{\zeta}$.
$\Delta P_k^{C,obj}$	Objective amount of active power to be shifted from Ω_k^C to Ω_k^R for IM k.

D. FUNCTIONS

$\boldsymbol{\zeta}$	Probability density function of fault occurrence for each transmission line.
$H(\cdot)$	Function that describes ρ_k (CCT $> \alpha_k$).

I. INTRODUCTION

POWER systems are expected to operate economically while maintaining the stability requirements of the grid. Appropriate restrictions prevent a system from suffering huge economic losses caused by transient instability resulting from different contingencies [1].

In such a context, optimal power flow (OPF) has been widely studied to address the economic side, followed by various methods to explore the solution for the transient stability constrained OPF (TSC-OPF) problem. Transient stability of a post-fault system is determined by solving a set of differential-algebraic equations (DAEs) that represent the system transients, and the power flow solution corresponds to the pre-fault operating point for solving the DAEs, which significantly affects the system stability. However, the DAE-constrained optimization problem cannot be solved directly. One of the most popular solutions is to discretize the DAEs into algebraic constraints by small time steps and then apply nonlinear programming techniques [2], [3]. Another prevalent method is trajectory sensitivity-based techniques, which iteratively adjust the dispatch based on the sensitivity of the stability index of interest to system control variables with the aid of time-domain simulations (TDSs) [4], [5]. The evolutionary algorithm-based technique is also a feasible approach that seeks the optimal solution of the TSC-OPF problem via mechanisms inspired by biological evolution [6], [7]. In addition to these methods, the machine learning (ML)-incorporated method is another popular solution for solving the TSC-OPF problem. In [8], a neural network is utilized to generate a preventive control solution, in which the sensitivities between the stability margin and output of each generator are obtained from the trained neural network. In [9], a hybrid method combining support vector machine and TDS is proposed, in which the relations of the support vector machine-based stability index with respect to control variables are calculated to find the TSC-OPF

solution. In [10] and [11], decision tree is applied to build the security boundaries and then the expected dispatching solution is searched within the feasible region. In [12], a deep belief network-based framework is developed to produce the optimal preventive control strategy. Regardless of their pros and cons, these works mainly focus on deterministic systems. However, they face challenges when applied to high renewable energy-integrated systems.

First, multi-source renewables such as wind power are highly variable even within a single hour [13]. Given that OPF is frequently solved for the hour-ahead system [14], numerous possible system operating points need to be considered in each power dispatch. This results in an unacceptable computational burden for deterministic approaches.

In addition, stochastic factors such as wind power in power systems affect transient stability [15]; so, it is necessary to analyze the transient stability from a probabilistic point of view. In previous studies, a point estimate method and Kalman filter are respectively applied in [16] and [17] to estimate the uncertainty of the system stability margin caused by the wind power uncertainties; in [18], Taguchi's orthogonal array testing is utilized to solve the TSC-OPF problem considering wind power variations. Although these methods dramatically reduce the test scenarios, the influence of wind power uncertainty on stability may not be fully considered. Moreover, the accuracy of the estimation may degrade if the wind generation does not follow the predetermined probability distribution.

Moreover, existing TSC-OPF studies mainly handle a limited set of fault scenarios. Given the probabilistic nature of different contingencies, a dispatching method that sets flexible probabilistic stability standards against various contingencies is rarely addressed in the literature and can be beneficial to evaluate the overall stability of the system.

To unravel the above-mentioned restrictions, a novel power dispatching method is put forward. First, instability mode (IM)-categorized probabilistic transient stability constraints (PTSCs) are formulated for all transmission lines that potentially trigger instability. Note the IM refers to the clustering of the critical and remaining generators. Next, to eliminate the need to run excessive time-consuming TDSs in each dispatching operation, an ML-based model is trained offline to predict the critical clearing time (CCT) and IM. Based on the predictions, the current system operation plan is evaluated with respect to the PTSCs, and the sensitivity of the probabilistic level of the CCT to the active power generated from the critical generators is calculated for each IM category. Accordingly, a set of dispatching constraints are generated and embedded into the conventional OPF formulation, and then the dispatch is rescheduled.

The main contributions of this paper are threefold:

1) IM-categorized PTSCs are formulated to facilitate the dispatching plan against various faults considering uncertainties and to enable operators to set flexible probabilistic stability levels for each IM to be prevented;

2) An ML technique is utilized, for the first time, to solve the power dispatch problem considering PTSCs. Compared to existing methods, the proposed approach can rapidly evaluate the stability status for a system considering uncertainties without reducing the test scenarios; and

3) The sensitivity of the probabilistic level of the CCT to the active power generated from the critical generators is proposed, whereby the PTSCs can be converted into a set of explicit dispatching constraints; thus, the dispatch is rescheduled to ensure the probabilistic stability requirements are met at an economical operating cost.

II. MATHEMATICAL FORMULATION
A. OBJECTIVE FUNCTION
The objective of generation scheduling is to minimize the total operating cost of synchronous generators (SGs).

$$\min \sum_{g \in \Omega^G} \left(a_{2g} P_g^2 + a_{1g} P_g + a_{0g} \right) \tag{1}$$

where a_{2g}, a_{1g}, and a_{0g} are the generation cost coefficients of the gth SG, P_g is the active power output of the gth SG, and Ω^G is the set of SGs.

B. STATIC CONSTRAINTS
AC power flow equations are described by (2), where Ω^B is the set of buses and $i \in \Omega^B$; P_i and Q_i are the active and reactive power injection from the SG at bus i, respectively; V_i is the voltage magnitude of bus i; P_{Wi} and Q_{Wi} are the active and reactive wind power injections at bus i, respectively; θ_{ij} is the voltage angle difference between bus i and j; P_{Di} and Q_{Di} are the active and reactive loads at bus i, respectively; and G_{ij} and B_{ij} are conductance and susceptance between buses i and j, respectively.

$$\begin{cases} P_i + P_{Wi} - P_{Di} - V_i \sum_{j \in \Omega^B} V_j \left(G_{ij}\cos\theta_{ij} + B_{ij}\sin\theta_{ij} \right) = 0 \\ Q_i + Q_{Wi} - Q_{Di} - V_i \sum_{j \in \Omega^B} V_j \left(G_{ij}\sin\theta_{ij} - B_{ij}\cos\theta_{ij} \right) = 0 \end{cases} \tag{2}$$

$$\begin{cases} \underline{P_g} \le P_g \le \overline{P}_g, & g \in \Omega^G \\ \underline{Q_g} \le Q_g \le \overline{Q}_g, & g \in \Omega^G \\ \underline{V_i} \le V_i \le \overline{V}_i, & i \in \Omega^B \\ \underline{\theta_i} \le \theta_i \le \overline{\theta}_i, & i \in \Omega^B \\ \underline{I_l} \le I_l \le \overline{I}_l, & l \in \Omega^L \end{cases} \tag{3}$$

Equation (3) denotes the constraints of bus power injection, bus voltage magnitudes, and line current magnitudes, where θ_i is the angle of bus voltage, I_l is the current on line l, and Ω^L is the set of transmission lines.

C. DYNAMIC CONSTRAINTS

$$\begin{cases} \dot{x}(t) = \mathbf{D}(x(t), y(t), u, \varepsilon) \\ \mathbf{E}(x(t), y(t), u, \varepsilon) = 0 & t \in [t_0, t_{end}] \\ x(t_0) = x_0, y(t_0) = y_0 \end{cases} \tag{4}$$

The dynamic equations are listed in (4), where $x(t)$ and $y(t)$ are respectively the state and algebraic variables in the transient period $[t_0, t_{end}]$ with initial values $\mathbf{x}_0$ and $\mathbf{y}_0$ at t_0; t_{end} is the end time of transients. u includes control variables such as the active power output of each SG, ε includes uncertainties that affect the system operating point, e.g., variations of the power generated from each wind power plant (WPP), etc. $\mathbf{D}(\cdot)$ is the differential equations representing system transients and $\mathbf{E}(\cdot)$ is the power balance equations to be satisfied at each instant of time.

In this study, SGs in the networks are round rotor generator model GENROU equipped with IEEEX1 excitation systems. IEEEST stabilizers and IEESGO governors are installed for each SG. Each WPP is modeled by an aggregated 1.5 MW doubly-fed induction generator model. Note that the dynamic constraints given by (4) are not directly formulated in the power dispatching formulation. Instead, they are considered inside the dynamic simulations during the database generation stage. Thus, the dynamics of the system can be learned by the prediction model, which is then applied to online dispatching operations. More details about the prediction model are discussed in Section III.

D. PROBABILISTIC TRANSIENT STABILITY CONSTRAINTS
Generally, the PTSC of a power system can be formulated as [16]:

$$\rho \left(\tau \left((x_{sol}, y_{sol}), \Omega^L, \zeta, u, \varepsilon, T \right) > \alpha \right) \ge \beta \tag{5}$$

where $\rho(\cdot)$ represents the probability; τ is the stability index of interest, which is the CCT in this paper but any other stability index such as the stability margin can be used in a straightforward manner; and (x_{sol}, y_{sol}) represents a dispatching solution, i.e., the system state and algebraic variables after a certain dispatch. ζ is the probability density function (PDF) of fault occurrence for each transmission line in Ω^L and T is the time interval between two consecutive dispatching operations. Given that OPF is frequently solved for hourly operation [14], T is set to one hour in this research. α is the user-defined threshold value of the CCT. Constraint (5) states that if a random fault occurs at lines in Ω^L between two consecutive dispatching operations, considering ζ and ε during this period, the probability of CCT $> \alpha$ must not be less than the security level β.

Figures 1 and 2 are illustrative examples showing the idea of incorporating PTSCs into the power dispatch problem using a two-machine power system. Fig. 1 shows two dispatching solutions and their corresponding possible operating points in an interval T, in which the two solutions are calculated from OPF with and without PTSCs. Fig. 2 depicts the PDF of the CCT of the two solutions with respect to a set of potential faults, in which the violation area corresponds to the possibility that the CCT is below the threshold value α. The two figures convey the idea that, by incorporating PTSCs into power dispatch, the stability level of the system is expected to satisfy the security requirement.
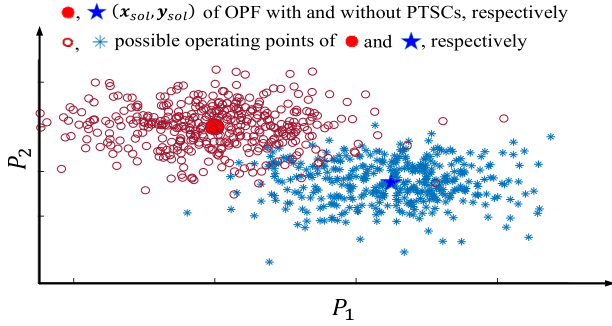
FIGURE 1. Illustration of the power dispatch with and without PTSCs.
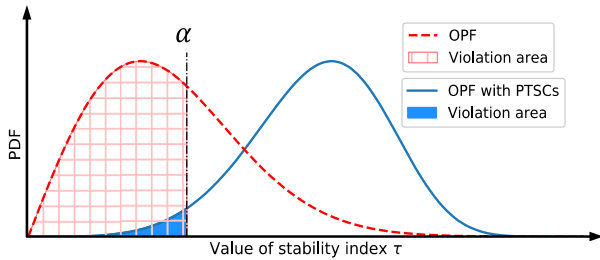
FIGURE 2. PDF of the stability index with and without PTSCs.

However, it is cumbersome to analyze each potential fault individually after considering ε, and therefore dealing with (5) in the OPF problem can be complicated. In this regard, given that a certain dispatching solution may have a similar effect on system vulnerability to multiple faults that trigger the same IM [5], PTSCs are formed in a more generic and tractable manner by:

$$\rho\left(\text{CCT}\left(\left(x_{sol}, y_{sol}\right), \Omega^{\text{L}}, \zeta, u, \varepsilon, T\right) > \alpha_k\right)$$
$$\geq \beta_k \forall k \in \Omega^{\text{IM}} \quad (6)$$

where Ω^{IM} is the set of all IMs that may appear in the network. This manner also helps to set flexible probabilistic stability standards for each IM to be prevented. Note that IMs are similar to coherent groups of generators with the main exception that they only contain two clusters of generators, i.e., the critical SGs and the remaining ones [19], [20]. In the following, $\rho\left(\text{CCT}\left(\left(x_{sol}, y_{sol}\right), \Omega^{\text{L}}, \zeta, u, \varepsilon, T\right)\right) > \alpha_k$ is represented as $\rho_k\left(\text{CCT} > \alpha_k\right)$ for simplicity.

As the system operating cost may increase after considering the PTSCs, this paper aims to offer a computationally efficient dispatching method with a satisfactory trade-off between economics and stability.

III. THE PROPOSED SOLUTION

The proposed approach is elaborated in this section. First, the offline training and online application of the (CCT, IM) prediction model are introduced. A method that converts the PTSCs into linear algebraic form is then introduced, followed by a flowchart representing the proposed solution framework.

A. TRAINING OF THE (CCT, IM) PREDICTION MODEL

The CCT and IM are two important indices in power system transient stability analysis. The value of the CCT correlates the system stability level against a specific fault, and the identification of IM determines the critical SGs that lose synchronism.

Denote $\Omega^{\text{CCT,IM}}$ as a set of data pairs (CCT, IM) that contains the CCTs and IMs of a specific system under all possible fault scenarios. For a deterministic system under a set of preconceived faults, the $\Omega^{\text{CCT,IM}}$ can be collected by conducting TDSs for all possible fault scenarios. The $\Omega^{\text{CCT,IM}}$ reflects the overall stability level of a system and identifies the vulnerable SGs; this information provides system operators with the basis for preventive dispatch. However, for a high wind power-integrated system, collecting $\Omega^{\text{CCT,IM}}$ by TDSs is computationally inefficient as the potential operating points increase exponentially.

To address this issue, a prediction model is trained offline using an ML technique to rapidly predict the CCT and IM for a large number of possible fault scenarios. To this end, system pre-fault variables and fault locations, as listed in Table 1, are selected as input features for model training [21]. The data pair (CCT, IM) for each case is used as target labels.

The processes of database generation and ML-based model training are illustrated in the left part of Fig. 3. The training data are obtained from Monte Carlo TDSs. To obtain an adequate and reasonable training database, the statistical models of uncertainties, including outputs of each WPP, load levels, and fault locations, are estimated from their corresponding historical observations. Next, Monte Carlo TDSs are conducted: in each simulation, the uncertain variables in the system are sampled from the corresponding statistical models. Then, the selected features and target labels (CCT and IM) are extracted from the simulation results and saved in the database. After the database is generated, a prediction model is trained and saved for online applications. Note that the database generation and training process are performed offline and do not increase the computational time during the online application.

Specifically, the prediction model consists of a regression model (to predict CCT) and a multi-class classification model (to predict IM). In this research, an ensemble technique that combines multiple classification and regression trees [22] trained by the adaptive boosting (AdaBoost) method [23] is applied. AdaBoost is an ML meta-algorithm used in conjunction with many other types of learning algorithms and can be applied to multi-class classification [24] and regression problems [25].

For the multi-class classification problem, the AdaBoost technique fits a sequence of weak classifiers on repeatedly modified versions of the data. The data modifications at each so-called boosting iteration apply weights $\eta_1, \eta_2, \ldots, \eta_N$ to each of the total training samples, where N is the number of total training samples. Initially, those weights are all set to $1/N$ so that the first step simply trains a weak learner on the original data. At each step, misclassified training data

TABLE 1. Selected features for prediction model training.

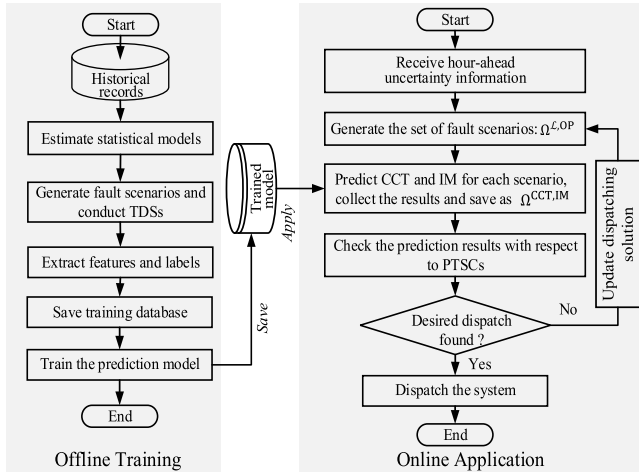| Feature	Description
1	Rotor angles of each SG
2	Fault location (categorical feature)
3	Active power output of each SG and WPP
4	Reactive power output of each SG

FIGURE 3. Offline training and online application of the ML-based model.

have their weights boosted, or decreased otherwise. As iterations proceed, examples that are difficult to predict receive ever-increasing influence. Each subsequent weak classifier is thereby forced to concentrate on the samples that are missed by the previous ones in the sequence. The final classifier is defined as the linear combination of the classifiers from each step.

Similarly, for the regression problem, regressors are trained sequentially. At each boosting iteration, a new regressor is fitted on a modified version of the original database and, based on the prediction results of the newly constructed regressor, the weights of those samples most in error are adjusted. As such, subsequent regressors focus more on difficult cases. All trained regressors are combined using the weighted median at the end of the training.

Detailed descriptions of AdaBoost for classification and regression are provided in [24] and [25], respectively. Other regression and classification techniques such as deep learning can also be applied without loss of generality.

B. ONLINE APPLICATION OF THE PREDICTION MODEL

The online application of the trained model is illustrated in the right part of Fig. 3. The purpose of the trained model in the online application stage is to rapidly assess the transient stability of a large number of possible fault scenarios during a dispatch. To generate these scenarios, the PDFs of fault locations and hour-ahead wind power uncertainty information are required. Such information is fairly accessible for operators in practice. Specifically, the PDF of fault locations,

ζ, which represents the probability that a fault occurs on any transmission line if a fault would occur in the system, can be set by system operators based on historical records. The hour-ahead wind power uncertainty of each WPP can be represented by a prediction interval (PI), which is prevalent in short-term wind power prediction and can provide ample uncertainty information [13]. Thus, the lists of fault lines L and a set of feasible wind power generation scenarios Ω^w can be generated by sampling from the ζ and PIs, respectively. Next, the set of possible operating points Ω^{OP} is generated based on Ω^w, where $|\Omega^{OP}| = |\Omega^w|$. Further, the set of fault scenarios, $\Omega^{L,op}$, which consider each fault at L for all operating points in Ω^{op}, are generated, where $|\Omega^{L,op}| = |L| \times |\Omega^{OP}|$. As a result, $\Omega^{CCT,IM}$ is predicted for $\Omega^{L,op}$ by the trained model.

Once the $\Omega^{CCT,IM}$ is collected, it will be checked with respect to PTSCs, i.e., the values of ρ_k (CCT > α_k) $\forall k \in \Omega^{IM}$ are calculated based on the $\Omega^{CCT,IM}$ and then compared to the PTSCs. To do this, the CCTs in $\Omega^{CCT,IM}$ are clustered into different groups based on their related IM. Thus, $\forall k \in \Omega^{IM}$, the PDF of the CCT, $\wp_k$(CCT), can be estimated based on the statistical data of the corresponding group. In this research, it is estimated using Gaussian kernels in a non-parametric way [26]. Then, the ρ_k (CCT > α_k) $\forall k \in \Omega^{IM}$ can be calculated by:

$$\rho_k\,(\text{CCT} > \alpha_k) = 1 - \int_0^{\alpha_k} \wp_k\,(\text{CCT})d\,(\text{CCT}) \qquad (7)$$

In this way, the stability status is checked with respect to PTSCs, and the dispatching plan will be rescheduled accordingly.

C. CONVERTING PTSCs INTO LINEAR ALGEBRAIC FORM

This subsection discusses the dispatching method. The transient stability level of the system against a specific IM can be improved by shifting the active power generated from Ω_k^C to Ω_k^R where Ω_k^C and Ω_k^R are the set of critical and remaining SGs in regard to IM k, respectively. The physical interpretation of this active power shift can be explained via the extended equal area criterion (EEAC) [19]. Based on the EEAC, Ω_k^C and Ω_k^R can be modeled by two equivalent SGs, and then be reduced to a one-machine-infinite-bus (OMIB) system, as shown in Fig. 4 (a)–(c). The dynamic mapping of the equivalent OMIB under such an IM is given by (8)–(10), where P, P_{mech}, and ω, are the active power, mechanical power, and angular speed of the equivalent OMIB, respectively; ω_0 is synchronous speed; M_C and M_R are equivalent inertia of Ω_k^C and Ω_k^R, respectively; and $P_{mech,g}$ is the mechanical power of the gth SG. Note that M_C and M_R are constants for a specific IM.

$$\frac{d\omega}{dt} = \frac{\omega_0\,(M_C + M_R)}{M_C M_R}(P_{mech} - P) \qquad (8)$$

$$P_{mech} = \frac{1}{M_C + M_R}$$
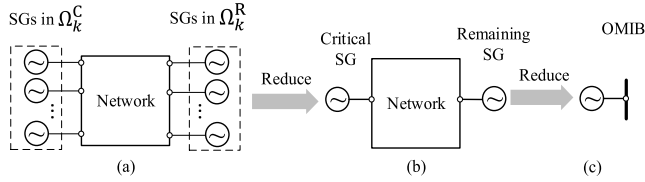
FIGURE 4. A system is reduced to OMIB.

$$\times \left(M_C \sum_{g\in\Omega_k^C} P_{mech,g} - M_R \sum_{g\in\Omega_k^R} P_{mech,g} \right) \tag{9}$$

$$P = \frac{1}{M_C+M_R} \left(M_C \sum_{g\in\Omega_k^C} P_g - M_R \sum_{g\in\Omega_k^R} P_g \right) \tag{10}$$

During a severe fault, P decreases drastically (assume $\approx$ 0) while P_{mech} remains at its steady-state value; as a result, $\frac{d\omega}{dt} > 0$, and the rotor angle of the OMIB increases during the fault. According to (8)–(10), shifting power from Ω_k^C to Ω_k^R functionally reduces the P and P_{mech} of the OMIB in steady state without changing the total power supply, thus helping to reduce the angular acceleration $\frac{d\omega}{dt}$ of the OMIB during the fault. Accordingly, the transient stability is reinforced for the specific IM. The same procedure can be applied to all IMs of interest in a straightforward manner.

In this research, it is assumed a quasi-linear relationship exists between the probabilistic transient stability level and the active power generated from Ω_k^C. According to this relationship, to satisfy the PTSCs as shown in (6), the amount of active power generation to be shifted from Ω_k^C to Ω_k^R can be calculated.

To show the relationship, $\forall k \in \Omega^{IM}$, it is assumed that:

$$\rho_k \left(CCT > \alpha_k\right) = H_k \left(\left(x_{sol}, y_{sol}\right), \Omega^L, \zeta, \tilde{u}, \varepsilon, T, u \right) \tag{11}$$

where $\tilde{u}$ includes all of the control variables except u. $H_k (\cdot)$ is the implicit expression of $\rho_k (CCT > \alpha_k)$ and reveals the variables that affect the value of $\rho_k (CCT > \alpha_k)$. Linearizing the function with respect to u, and ignoring the high-order terms of the Taylor series expansion given the quasi-linear relationship, gives:

$$\Delta\rho_k \left(CCT > \alpha_k\right) \approx \frac{\partial H_k \left(\left(x_{sol}, y_{sol}\right), \Omega^L, \zeta, \tilde{u}, \varepsilon, T, u \right)}{\partial u} \Delta u \tag{12}$$

where $\frac{\partial H_k}{\partial u}$ is the sensitivity of $\rho_k (CCT > \alpha_k)$ to u. Now, taking P_k^C as u, and ΔP_k^C as Δu, gives:

$$\begin{aligned} &\Delta\rho_k \left(CCT > \alpha_k\right) \\ &\approx \frac{\partial H_k \left(\left(x_{sol}, y_{sol}\right), \Omega^L, \zeta, \tilde{u}, \varepsilon, T, P_k^C \right)}{\partial P_k^C} \Delta P_k^C \end{aligned} \tag{13}$$

where P_k^C is the power generated from Ω_k^C:

$$P_k^C = \sum_{g\in\Omega_k^C} P_g \tag{14}$$

and because the change of P_k^C, i.e., ΔP_k^C, is the power shifted from Ω_k^C to Ω_k^R, ignoring the variation of transmission loss after power shifting, there is

$$\Delta P_k^C = \sum_{g\in\Omega_k^C} P'_g - \sum_{g\in\Omega_k^C} P_g \approx \sum_{g\in\Omega_k^R} P_g - \sum_{g\in\Omega_k^R} P'_g \tag{15}$$

After shifting the power, the change of ρ_k $(CCT > \alpha_k)$ can be calculated from:

$$\Delta\rho_k \left(CCT > \alpha_k\right) = \rho_k \left(CCT > \alpha_k\right) - \rho'_k \left(CCT > \alpha_k\right) \tag{16}$$

where $\cdot$ represents the corresponding variables before the power shifting. Thus, based on (12), the sensitivity of $\rho_k (CCT > \alpha_k)$ to the active power shift from Ω_k^C to Ω_k^R can be estimated by:

$$\begin{aligned} \xi_k &= \frac{\partial H_k \left(\left(x_{sol}, y_{sol}\right), \Omega^L, \zeta, \tilde{u}, \varepsilon, T, P_k^C \right)}{\partial P_k^C} \\ &\approx \frac{\Delta\rho_k \left(CCT > \alpha_k\right)}{\Delta P_k^C} \end{aligned} \tag{17}$$

Based on the assumed quasi-linear relationship, to achieve the stability level required (6), $\forall k \in \Omega^{IM}$, the objective amount of active power $\Delta P_k^{C,obj}$ to be shifted from Ω_k^C to Ω_k^R is calculated by:

$$\Delta P_k^{C,obj} = \frac{\beta_k - \rho_k \left(CCT > \alpha_k\right)}{\xi_k} \tag{18}$$

and then the dispatching plan against the faults is:

$$\forall k \in \Omega^{IM}, \quad \sum_{g\in\Omega_k^C} P'_g - \sum_{g\in\Omega_k^C} P_g \geq \Delta P_k^{C,obj} \tag{19}$$

Thus, the probabilistic stability constraints are transformed from (6) to (19), and are added to the conventional OPF formulations, as shown in (1)–(4). Finally, the OPF with PTSCs is solved, and the dispatching solution is updated. In this way, the power adjustment demand $\Delta P_k^{C,obj} \forall k \in \Omega^{IM}$ can be satisfied at the lowest total increment of the operating cost.

To correct the error from the quasi-linear relationship and avoid unnecessary over-stabilized situations (i.e., unnecessary cost increases due to excessive compliance with the PTSCs), the calculation and the shifting of $\Delta P_k^{C,obj}$ are executed iteratively until the expected dispatching solution is found.

It may be helpful to mention that the solution obtained by the proposed method is suboptimal. This is because it is difficult (if possible) to calculate the sensitivities of $\rho_k (CCT > \alpha_k)$ to the active power generated from each individual generator. Therefore, the sensitivity of $\rho_k (CCT > \alpha_k)$ to the active power generated from Ω_k^C is calculated instead, which then helps to convert the PTSC into explicit dispatching constraints.

D. THE OVERALL PROCESS OF THE PROPOSED SOLUTION ALGORITHM

The overall process of the proposed solution framework is illustrated in Fig. 5, where m is the iteration number, and M is the maximum allowed number of iterations. Before starting the iteration loop, the parameters for dispatching should be first set (step ① in the figure), followed by the generation of the Ω^{w} according to the hour-ahead PIs of each WPP (step ②). At each iteration, the dispatching solution $(\mathbf{x}_{sol}, \mathbf{y}_{sol})$ is first updated, followed by generation of the Ω^{OP} and $\Omega^{\mathrm{L,op}}$ (step ④). Next, the $\Omega^{\mathrm{CCT,IM}}$ is predicted for $\Omega^{\mathrm{L,op}}$ by the trained model, and the values of $\rho_k\,(\mathrm{CCT} > \alpha_k)\,\forall k \in \Omega^{\mathrm{IM}}$ are calculated (step ⑤), as introduced in Section III.B. Then, the constraints in (6) are checked (step ⑥). If all of the constraints in (6) are satisfied at the first iteration, i.e., the conventional OPF solution already meets the PTSCs, then no further action is needed (steps ⑦ to ⑨). Otherwise, the current plan needs to be rescheduled against instabilities or to avoid unnecessary over-stabilized situations. In this regard, $\forall k \in \Omega^{\mathrm{IM}}$, (14)–(19) are carried out to convert the PTSCs into a set of linear inequality constraints (step), during which the ξ_k in (17) can be calculated from two successive iterations. Specifically, at the first iteration, no power has been shifted from Ω_k^{C} to Ω_k^{R}; so, (14)–(18) are inexecutable. Thus, $\Delta P_k^{\mathrm{C,obj}}\forall k \in \Omega^{\mathrm{IM}}$ can be initialized to $\varphi \sum_{g \in \Omega_k^{\mathrm{C}}} P_g$ (step ③), where φ is a value between 0 and 1. The transformed linear inequality constraints (19) are then created (if $m = 2$) or updated (if $m > 2$) and added to the OPF formulation.

Notably, for over-stabilized situations, which may happen during iterations:

$$\exists \rho_k\,(\mathrm{CCT} > \alpha_k) > \beta_k \forall k \in \Omega^{\mathrm{IM}} \tag{20}$$

a negative $\Delta P_k^{\mathrm{C,obj}}$ would be obtained from (18) for corresponding k. Then, according to (19), the power output constraints for the SGs in Ω_k^{C} can be relaxed to allow some active power shift from Ω_k^{R} back to Ω_k^{C}; thus, a more cost-saving dispatching result can possibly be found.

The iteration is terminated when all constraints in (6) are satisfied and, at the same time, the maximum power output change in all SGs between the current and last iteration is less than a threshold value $\underline{\Delta P}$:

$$\Delta P_g^{\max} \leq \underline{\Delta P} \tag{21}$$

where

$$\Delta P_g^{\max} = \max \left| P_g' - P_g \right| \forall g \in \Omega^{\mathrm{G}} \tag{22}$$

Therefore, the dispatching plan is finalized when both (6) and (21) are satisfied. Otherwise, the flowchart enters the next iteration, the dispatching solution is updated, and the new iteration proceeds, as shown in Fig. 5.

IV. TEST AND RESULTS

The described framework is realized by a Python-based interface that calls PSS/E software to conduct dynamic simulations, save the data for training and testing of the prediction
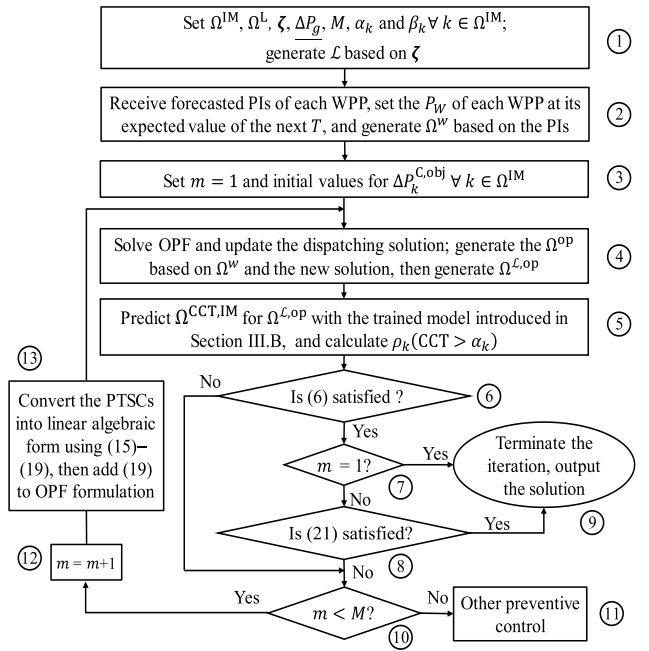

FIGURE 5. Flowchart of the proposed framework.

model; the prediction model is trained using the *scikit-learn* 0.20.4 package [27] in Python 2.7.15. Next, the interface implements the proposed procedure, during which the OPF is solved with the converted PTSCs at each iteration.

The IEEE 68-bus, 16-machine network is employed and modified to perform the simulations. The configuration of the network is omitted herein and can be found in [28]. Nine WPPs are installed at bus-18, −22, −25, −29, −31, −32, −36, −41, and −42 in the network, and the installed capacity of each is 800 MW; thus, the wind power installed capacity accounts for 40% of the gross load. The dynamic models adopted in the network are noted in Section II.C. The dynamic parameters of the SGs and WPPs are listed in [29], and all the dynamic models are available in [30]. The computer used in simulations featured an Intel 3.4-GHz CPU with 16 GB of RAM.

A. TRAINING AND TESTING OF THE (CCT, IM) PREDICTION MODEL

Database generation is required to train the prediction models. The training database is obtained from Monte Carlo TDSs. In this regard, reasonable uncertainty models, including outputs of WPPs and load levels, are essential. In practice, these uncertainty models can be statistically estimated from the corresponding historical observations. In this study, the historical wind and load data for the past five years (2016∼2020) are obtained from [31] and [32], respectively. Then, the PDFs of the power generation of each WPP and load level are generated based on the corresponding historical data using Gaussian kernels in a non-parametric way [26]. Thus, at each TDS during the generation of the database,

TABLE 2. Time consumption and performance of the prediction model.

Database generation	Prediction for CCT	Prediction for IM
66406 s	MSE: 1.3440×10^{-4}	Accuracy: 99.17%

TABLE 3. IMs to be prevented and the fault lines considered in dispatching.

k	IM details (Ω_k^C/Ω_k^R)	Ω^L
1	(SG16)/(SG1-15)	
2	(SG14-16)/(SG1-13)	(lines between bus-bus)
3	(SG6-7)/(SG1-5, SG8-16)	18-42, 18-49, 18-50, 21-22,
4	(SG9)/(SG1-8,SG10-16)	21-68, 25-26, 25-54, 26-27,
5	(SG8-9)/(SG1-7, SG10-16)	26-28, 26-29, 27-37, 27-53,
6	(SG11)/(SG1-10, SG12-16)	28-29, 32-33, 37-52, 37-68,
7	(SG4-7)/(SG1-3, SG8-16)	40-41, 41-42, 45-51, 50-51
8	(SG14)/(SG1-13, SG15-16)	

TABLE 4. α_k and β_k set for dispatching.

k	1	2	3	4	5	6	7	8
α_k (s)	0.10	0.10	0.20	0.15	0.15	0.16	0.20	0.15
β_k (%)	95 $\forall k \in \Omega^{IM}$							

TABLE 5. Selected one hour wind power data.

WPP	Selected time period	Output*	WPP	Selected time period	Output*
1	01/06/19 00:25–01:25	475.81	6	11/20/17 15:55–18:55	527.91
2	03/25/19 21:10–22:10	366.85	7	02/17/16 20:20–21:20	330.90
3	05/25/18 23:25–24:25	472.82	8	03/06/16 13:50–14:50	323.31
4	10/28/18 16:50–17:50	322.72	9	10/10/16 00:50–01:50	321.97
5	11/28/17 16:50–17:50	551.41	Time format: (MM/DD/YY hr:min)		

*Expected (average) output (MW) of each WPP in the following hour

the load level and WPP outputs are sampled from their respective PDFs. Next, the active power outputs of each SG are randomly dispatched in their respective output limits, such that the total demand and generation are balanced. Subsequently, a fault is randomly applied to transmission lines. The faults are assumed to be permanent and are cleared by switching out the faulted line. Only three-phase faults are considered in this paper, though the proposed method is also capable of handling other fault types. The selected features (listed in Table 1) and the target labels (CCT, IM) obtained from each simulated case are saved into the database. The TDSs are conducted until the generation of the database is completed.

Finally, 60,000 cases are generated by running TDSs. Given the fault clearing time of a breaker is typically less than 0.2 s [33], the range of CCT values considered in the simulation is between 0 and 0.25 s; i.e., a fault with a CCT that is larger than 0.25 s can be considered safe as it can be cleared by a breaker before the system reaches a critical condition. 5-fold cross-validation is adopted for model testing. The training time and test accuracy of the prediction model are reported in Table 2, where the test accuracy includes the mean squared error (MSE) of CCT prediction and the classification accuracy of IM prediction. The results validate the high accuracy of the trained model with respect to predictions of CCT and IM. The trained model will be applied to dispatching operations in Section IV.B.

It is worth noting that, as a by-product of the model training stage, eight prominent IMs of the system are detected and listed in Table 3. Thus, the set of IMs, $\Omega^{IM} := \{k = 1, 2, \ldots, 8\}$, and the system will be dispatched against these IMs in the following subsection. To keep the dispatch more focused on critical lines, only fault lines with instability-triggering records during the TDSs are selected to recompose the Ω^L, as listed in Table 3.

B. TEST OF THE PROPOSED FRAMEWORK

The settings of Ω^{IM}, Ω^L, ζ, ΔP_g, M, α_k, and $\beta_k \forall k \in \Omega^{IM}$, and hour-ahead PIs for each $\overline{WPP}$ are required to conduct

the test, as shown in steps ①– ② in Fig. 5. The settings of Ω^{IM} and Ω^L have been introduced in Section IV.A. The ζ is set to uniform distribution, and thus the L is set equal to the Ω^L in this situation. The $\underline{\Delta P}$ is set at 5 MW, which is 0.1% of the upper output limit of the largest SG in the network; and M is set at 10. However, these parameters can be set to any other values without loss of generality. The α_k and $\beta_k \forall k \in \Omega^{IM}$ are listed in Table 4. Specifically, the security levels $\beta_k \forall k \in \Omega^{IM}$ are set at 95% as a trade-off between economics and stability. In practice, the system operators can also use the proposed method to set the probabilistic transient stability level at different values (e.g., 80–100%) based on practical requirements. Other settings above can also be adjusted according to different dispatching requirements.

In addition, to set the assumed hour-ahead PIs for all WPPs in the modified IEEE 68-bus network, nine sets of hourly wind power data with a 5-minute resolution are selected from [31], and then a prediction interval for each data series is produced based on ±10% of the recorded value. The selected data and the corresponding PI curves are shown in Table 5 and Fig. 6, respectively. Following that, 1200 wind power generation scenarios Ω^w are generated, i.e., 100 scenarios are randomly sampled every 5 minutes in the dispatching time interval based on the PIs. So far, the simulation parameters have been set (steps ①– ② in Fig. 5). Subsequently, the procedures in the proposed framework proceed until the terminate condition is met.

Tables 6 and 7 list the values of ρ_k (CCT $>\alpha_k$) $\forall k \in \Omega^{IM}$ and corresponding dispatching solution obtained from the proposed method at each iteration, respectively. It is worth noting that the solution of the first iteration, solved by conventional OPF, does not satisfy the PTSCs. The expected dispatching solution is found after eight iterations using the proposed method, during which the values of ρ_k (CCT $>\alpha_k$) $\forall k \in \Omega^{IM}$ increase and finally meet the security requirements (i.e., 95%). Notably, the operating cost of the proposed method only increased by 3.26% compared to OPF, as shown in Table 7.

The results demonstrate that using the assumed sensitivity in (17) is feasible for solving the power-dispatching problem

TABLE 6. Values (%) of ρ_k (CCT $>\alpha_k$) at each iteration.

k	Iterations							
	1st	2nd	3rd	4th	5th	6th	7th	8th
1	54.56	59.76	99.21	99.99	99.99	99.99	99.99	**99.99**
2	74.96	76.27	83.60	96.80	96.15	95.02	94.52	**95.11**
3	64.71	70.77	93.31	93.23	94.85	95.23	95.31	**95.30**
4	84.05	92.47	95.72	95.43	95.15	95.12	95.09	**95.06**
5	79.61	85.62	98.03	97.04	95.71	95.22	95.31	**95.29**
6	18.61	99.99	99.99	99.99	99.84	99.85	99.69	**98.61**
7	78.31	89.07	96.31	94.46	96.00	96.31	96.61	**96.61**
8	45.85	60.42	82.38	92.57	94.04	94.20	95.04	**95.02**

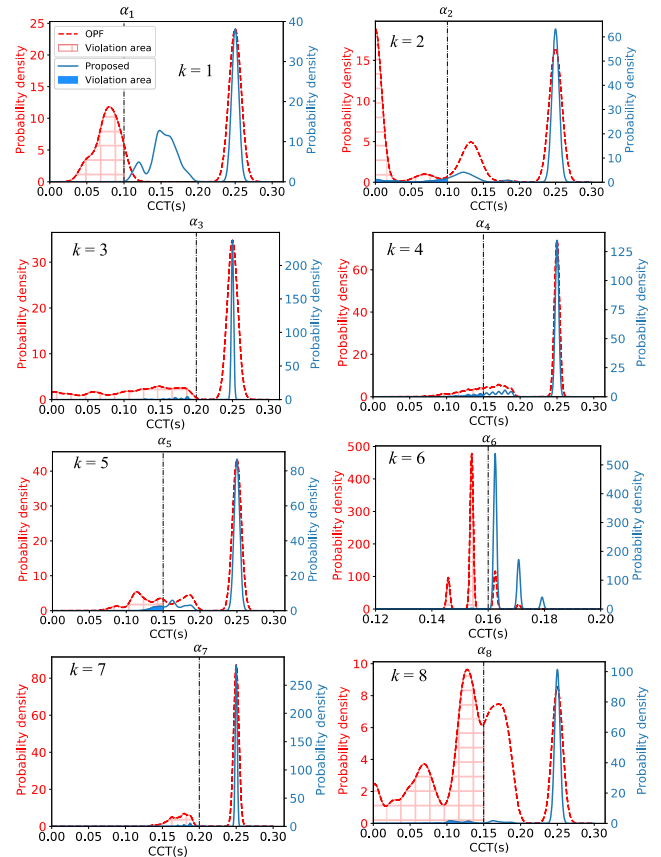**TABLE 7.** Active power output (MW) of each SG and operating cost at each iteration.

SG	Iteration							
	1st	2nd	3rd	4th	5th	6th	7th	8th
1	129.15	139.22	182.14	194.39	192.81	190.79	190.55	**190.42**
2	371.46	388.42	460.39	480.85	478.26	474.90	474.47	**474.26**
3	450.22	468.89	547.35	569.52	566.75	563.12	562.65	**562.41**
4	391.21	391.18	493.60	505.43	519.62	515.83	515.29	**514.81**
5	345.98	346.02	416.83	425.04	434.80	432.18	431.81	**431.48**
6	440.81	414.43	308.46	300.49	274.09	271.57	273.08	**273.51**
7	341.51	317.89	223.15	216.05	192.45	190.20	191.55	**191.93**
8	346.33	346.33	296.05	308.96	324.63	333.70	332.67	**332.45**
9	526.24	476.24	448.58	454.70	458.33	459.58	460.63	**461.41**
10	432.95	453.08	545.34	573.05	569.34	564.81	564.29	**564.01**
11	753.55	703.55	706.63	709.70	712.77	715.75	718.72	**721.61**
12	1177.89	1220.77	1419.97	1479.28	1471.15	1461.32	1460.06	**1459.49**
13	2549.21	2635.68	3039.01	3158.95	3142.43	3122.51	3119.96	**3118.82**
14	1299.66	1249.66	1099.95	1013.91	993.43	979.99	961.31	**962.17**
15	739.43	778.21	627.45	596.01	606.97	616.79	620.77	**620.47**
16	3859.35	3809.35	3259.84	3077.31	3127.83	3174.66	3190.11	**3188.83**
k\$/h	106.63	106.74	109.08	110.31	110.32	110.14	110.12	**110.11**
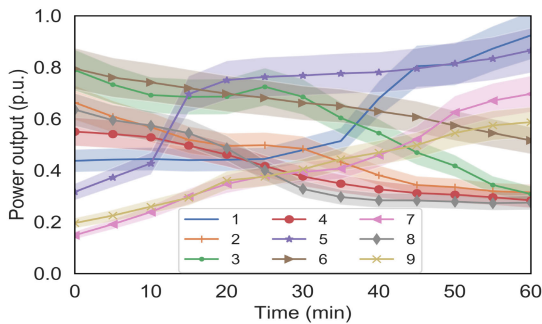
FIGURE 6. Hour-ahead wind power PI for each WPP.

FIGURE 7. Comparison of the probability distribution of CCT $\forall k \in \Omega^{IM}$.

considering PTSCs. In addition, the results show that the proposed method can handle unnecessary over-stabilized situations, e.g., in Table 6, the values of the ρ_k (CCT $>\alpha_k$) for $k = 2, 4, 5$, and 6 at the 4th iteration excessively satisfy the β_k, and this issue is alleviated at the following iteration. Accordingly, the operating cost decreases from 110.31 k\$/h to 110.11 k\$/h, as shown in Table 7.

Further, Fig. 7 visually compares the probability distributions of CCT $\forall k \in \Omega^{IM}$ before and after applying the proposed method. Specifically, the non-violation areas under each dashed curve correspond to the column values of the 1st iteration in Table 6, and the non-violation areas under

each solid curve correspond to the column values of the 8th iteration in Table 6. The figure shows that the violation areas are greatly reduced by applying the proposed method.

C. VALIDATING THE RESULTS USING TDSs

To verify the dispatching result of the proposed method, two validation tests are carried out: (1) the stability status of the dispatching result is tested by TDSs; and (2) the dispatching solution obtained from TDSs is also investigated, i.e., wherein the $\Omega^{CCT,IM}$ in step ⑤ of Fig. 5 is obtained from TDSs instead of the ML-trained model.

For (1), Table 8 lists the validation results and shows that the values of ρ_k (CCT $>\alpha_k$) verified by TDSs are quite close to the values output from the proposed method (listed in the last column of Table 6). Although the values of the ρ_k (CCT $>\alpha_k$) for $k = 4$ and 5 are slightly below 95% by 0.04 and 0.23%, respectively, the error is acceptable from an engineering point of view.

For (2), the simulation results based on TDSs are listed in Table 9. It reveals the dispatching solution and stability levels by the proposed method (listed in the last column of Table 6 and Table 7) are very close to those based on TDSs. In addition, a comparison of the two methods in terms of time consumption and the number of iterations is given in Table 10.

**TABLE 8. Values (%) of ρ_k (CCT $>\alpha_k$) tested by TDSs.**

k	1	2	3	4	5	6	7	8
Verified by TDSs	99.97	95.02	96.46	94.96	94.77	98.92	97.37	95.08

TABLE 9. Dispatching result and values of ρ_k (CCT $>\alpha_k$) based on TDSs.

Dispatching result (MW)							
SG	1	2	3	4	5	6	7	8
Output	192.14	477.02	565.44	518.34	433.91	283.68	201.02	297.02
SG	9	10	11	12	13	14	15	16
Output	449.43	567.28	720.73	1466.40	3132.73	969.38	617.19	3173.33
Final operating cost: 110.20 k$/h							
Values of ρ_k (CCT $> \alpha_k$) for each IM							
IM	1	2	3	4	5	6	7	8
Value (%)	99.94	95.05	95.01	95.14	95.06	95.02	95.76	95.00

TABLE 10. Time consumption and number of iterations for the two methods.

Method	Time consumed (s)	Iterations
TDS-based	186188	7
Proposed	287	8
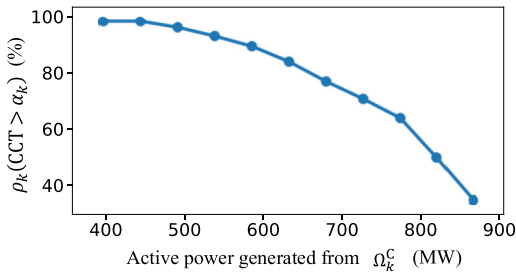
FIGURE 8. The value of ρ_k (CCT $>\alpha_k$) vs. the active power generated from Ω_k^C.

Notably, the proposed method is $186188/287 \approx 648$ times faster. This is because, for each iteration, $\left|\Omega^{L,op}\right| = 20 \times 1200 = 24,000$ cases are simulated by TDSs given $|\Omega^{op}| = 1200$ and $|L| = 20$ ($L = \Omega^L$ in this test), which may take an extensive amount of time. In contrast, the proposed method only needs to solve the power flows to generate the Ω^{op}. Then, the $\Omega^{CCT,IM}$ are accurately and rapidly predicted by the trained model. Thus, the calculation process takes less than 5 minutes, which is quite acceptable for hour-ahead operations.

The comparisons validate the good performance of the proposed framework in terms of practicability, searching for economical solutions, and computational efficiency. Given that most TSC-OPF works [4]–[5], [7], [16], [18] rely on TDSs and thus may have difficulty handling massive fault scenarios, the proposed method has more advantages for dealing with networks with high wind power penetration.

In addition, to justify the quasi-linear relationship in (12), the values of ρ_k (CCT $>\alpha_k$) with respect to the active power

TABLE 11. Dispatching result and values of ρ_k (CCT $>\alpha_k$) of the method in [18].

Dispatching result (MW)							
SG	1	2	3	4	5	6	7	8
Output	206.94	501.90	592.56	523.98	437.88	256.60	176.86	377.71
SG	9	10	11	12	13	14	15	16
Output	374.55	599.44	698.13	1534.98	3270.93	957.70	544.54	3000.00
Final operating cost: 111.91 k$/h							
Values of ρ_k (CCT $> \alpha_k$) for each IM							
IM	1	2	3	4	5	6	7	8
Value (%)	100.00	97.89	98.26	99.23	95.83	99.99	97.30	95.00

generated from Ω_k^C are simulated and reported in Fig. 8. In this test, an IM ($k = 3$) is selected, where the Ω_k^C includes SG6 and SG7, and the α_k is set at 0.2 s. Note that the change of the active power of Ω_k^C is balanced by SGs in Ω_k^R during the simulation. Fig. 8 shows a quasi-linear relationship exists between ρ_k (CCT $>\alpha_k$) and the active power generated from Ω_k^C. Similar simulation results can be obtained for other IMs.

D. COMPARISON WITH A STATE-OF-THE-ART METHOD
To further validate the advantage of the presented work, the dispatching solution of the proposed method is compared to that of a state-of-the-art method reported in [18]. In [18], a robust dispatch is proposed for power systems against transient instability considering highly variable and stochastic wind power generation. In this method, Taguchi's orthogonal array is utilized to select a small number of representative testing scenarios, thus dramatically reducing the computation time. The results and time consumptions of this method are reported in Table 11.

Compared to the results by the proposed method (listed in the last column of Table 6 and Table 7), the robust dispatch method from [18] yielded a relatively conservative solution, as most of the PTSCs (95%) are over-satisfied; therefore, the operating cost reaches 111.91 k$/h. In contrast, the operating cost associated with the proposed method is 110.11 k$/h.

In addition to the economic advantages, another benefit of the proposed method is that it enables operators to set different probabilistic stability levels (e.g., 80~100%) to each IM that needs to be prevented, which helps operators set more flexible dispatching plans.

E. VALIDATION OF THE FRAMEWORK ON THE IEEE 300-BUS NETWORK
The proposed method is also tested on the IEEE 300-bus network [34], which has 69 SGs and 304 transmission lines. Fifteen WPPs are installed at bus-84, -143, -190, -236, -241, -7002, -7003, -7012, -7017, -7024, -7039, -7061, -7130, -7139, and -7166, and the installed capacity of each is 800 MW. The wind power installed capacity accounts for 50% of the gross load.

The training and testing process described in Section IV.A is applied to train the (CCT, IM) prediction model, during which 152,000 cases are generated by TDSs. The

TABLE 12. Selected IM patterns, Ω^L, and the α_k and β_k Set for dispatching.

k	IM details (Ω_k^C)	α_k (s)	β_k (%)	Ω^L
1	(7166)	0.20		
2	All SGs except (63)	0.20		
3	(119)	0.15		(lines between bus-bus)
4	(119, 124)	0.15		62-64, 119-120, 119-121,
5	(185)	0.15	95	134-184, 140-182, 162-164,
6	(7139)	0.15		162-165, 163-164, 165-166,
7	(190)	0.15		190-231, 191-192, 191-225,
8	(191)	0.15		214-215
9	(213, 242, 243)	0.20		

TABLE 13. Selected one hour wind power data.

WPP	Selected time	Output*	WPP	Selected time	Output*
10	10/16/16 15:10–16:10	211.19	13	03/24/15 04:35–05:35	491.56
11	11/28/17 16:50–17:50	308.34	14	02/07/15 17:20–18:20	398.50
12	11/20/17 15:55–16:55	89.18	15	08/29/15 05:35–06:35	186.07

*Expected (average) output (MW) of each WPP in the following hour

TABLE 14. Comparison of different methods.

IM	Value (%) of ρ_k(CCT > α_k)		
	OPF ($m = 1$)	Proposed method	TDS-based
1	81.57	96.15	95.18
2	0.00	100	100
3	42.85	95.92	95.53
4	15.43	100	99.68
5	1.57	100	100
6	40.60	95.71	95.11
7	27.69	95.29	95.04
8	0.00	96.06	95.13
9	14.64	96.69	95.38
	OPF ($m = 1$)	Proposed	TDS-based
k\$/h	521.72	527.56	527.07
Time consumed (s)	–	549	174675
Iterations	–	12	9

computational time for database generation is 187,163 s. Based on the testing results, the MSE of the prediction for the CCT and the accuracy of the prediction for IM are 1.6107×10^{-4} and 99.39%, respectively. The results confirm the high accuracy of the trained model.

For the validation of the framework, nine IMs are selected, as listed in Table 12, in which the set of selected fault lines Ω^L, as well as α_k and β_k for dispatching, are also noted. M is set at 15. In addition, the wind power datasets listed in Tables 5 and 13, which are selected from [31], are used to set the assumed hour-ahead PIs for all WPPs. The procedure for setting PIs and other testing parameters is the same as that in Section IV.B.

Table 14 lists the simulation results solved by the proposed method, OPF (without considering the PTSCs), and the TDS-based method. It shows that the expected dispatching solution is found after 12 iterations utilizing the proposed method, in which the operating cost only increased by 1.12% with respect to the result of OPF. The table also shows that the final operating cost and stability levels of the proposed and TDS-based method are very similar, while the proposed method is $174675/549 \approx 318$ times faster. The results and comparison verify the effectiveness of the proposed method.

The test shows that the proposed method can be applied to power systems of different scales. Although the time consumption for a larger scale system may increase, it should not be a problem given that the proposed method is for hour-ahead dispatching operations, and no TDSs are required due to the incorporation of the ML-based prediction model.

V. CONCLUSION

This paper proposes a novel power dispatch method for high wind power-integrated systems considering PTSCs. First, a set of IM-categorized PTSCs are constructed to consider a large number of fault scenarios and to set flexible probabilistic stability margins for each IM to be prevented. Next, to overcome the necessity of running massive TDSs, a highly efficient ensemble learning-based model is trained and incorporated to predict the CCT and IMs for possible fault scenarios during dispatch. In addition, a method is put forward to convert the PTSCs into explicit dispatching constraints. Thus, based on the prediction, the PTSCs are converted into linear generation requirements and then embedded into conventional OPF formulation for dispatch rescheduling. The proposed method is suitable for considering bulk contingency scenarios scenarios caused by wind power uncertainty. The effectiveness of the proposed approach is validated on two IEEE test networks, and demonstrated superior performance in terms of providing high-quality solutions and computational efficiency.

Further research can be conducted to enhance the performance of the proposed method through different ML techniques. In addition, the framework may be improved to handle significant changes in the topology of the system and other situations such as under-frequency load shedding.

REFERENCES

[1] M. Rostami and S. Lotfifard, "Scalable coordinated control of energy storage systems for enhancing power system angle stability," *IEEE Trans. Sustain. Energy*, vol. 9, no. 2, pp. 763–770, Apr. 2018.

[2] D. Gan, R. J. Thomas, and R. D. Zimmerman, "Stability-constrained optimal power flow," *IEEE Trans. Power Syst.*, vol. 15, no. 2, pp. 535–540, May 2000.

[3] C.-J. Ye and M.-X. Huang, "Multi-objective optimal power flow considering transient stability based on parallel NSGA-II," *IEEE Trans. Power Syst.*, vol. 30, no. 2, pp. 857–866, Mar. 2015.

[4] A. Pizano-Martínez, C. R. Fuerte-Esquivel, E. A. Zamora-Cárdenas, and J. M. Lozano-García, "Directional derivative-based transient stability-constrained optimal power flow," *IEEE Trans. Power Syst.*, vol. 32, no. 5, pp. 3415–3426, Sep. 2017.

[5] Y. Xu, J. Ma, Z. Y. Dong, and D. J. Hill, "Robust transient stability-constrained optimal power flow with uncertain dynamic loads," *IEEE Trans. Smart Grid*, vol. 8, no. 4, pp. 1911–1921, Jul. 2017.

[6] H. R. Cai, C. Y. Chung, and K. P. Wong, "Application of differential evolution algorithm for transient stability constrained optimal power flow," *IEEE Trans. Power Syst.*, vol. 23, no. 2, pp. 719–728, May 2008.

[7] S. W. Xia, B. Zhou, K. W. Chan, and Z. Z. Guo, "An improved GSO method for discontinuous non-convex transient stability constrained optimal power flow with complex system model," *Int. J. Electr. Power Energy Syst.*, vol. 64, pp. 483–492, Jan. 2015.

[8] M. C. Passaro, A. P. A. da Silva, and A. C. S. Lima, "Preventive control stability via neural network sensitivity," *IEEE Trans. Power Syst.*, vol. 29, no. 6, pp. 2846–2853, Nov. 2014.

[9] F. Tian, X. Zhou, Z. Yu, D. Shi, Y. Chen, and Y. Huang, "A preventive transient stability control method based on support vector machine," *Electr. Power Syst. Res.*, vol. 170, pp. 286–293, May 2019.

[10] I. Genc, R. Diao, V. Vittal, S. Kolluri, and S. Mandal, "Decision tree-based preventive and corrective control applications for dynamic security enhancement in power systems," *IEEE Trans. Power Syst.*, vol. 25, no. 3, pp. 1611–1619, Aug. 2010.

[11] K. Sun, S. Likhate, V. Vittal, V. S. Kolluri, and S. Mandal, "An online dynamic security assessment scheme using phasor measurements and decision trees," *IEEE Trans. Power Syst.*, vol. 22, no. 4, pp. 1935–1943, Nov. 2007.

[12] T. Su, Y. Liu, J. Zhao, and J. Liu, "Deep belief network enabled surrogate modeling for fast preventive control of power system transient stability," *IEEE Trans. Ind. Informat.*, early access, Apr. 13, 2021, doi: 10.1109/TII.2021.3072594.

[13] J. Ma, M. Yang, and Y. Lin, "Ultra-short-term probabilistic wind turbine power forecast based on empirical dynamic modeling," *IEEE Trans. Sustain. Energy*, vol. 11, no. 2, pp. 906–915, Apr. 2020.

[14] R. Canyasse, G. Dalal, and S. Mannor, "Supervised learning for optimal power flow as a real-time proxy," in *Proc. IEEE Power Energy Soc. Innov. Smart Grid Technol. Conf. (ISGT)*, Apr. 2017, pp. 1–5.

[15] M. Edrah, K. L. Lo, and O. Anaya-Lara, "Impacts of high penetration of DFIG wind turbines on rotor angle stability of power systems," *IEEE Trans. Sustain. Energy*, vol. 6, no. 3, pp. 759–766, Jul. 2015.

[16] S. Xia, X. Luo, K. W. Chan, M. Zhou, and G. Li, "Probabilistic transient stability constrained optimal power flow for power systems with multiple correlated uncertain wind generations," *IEEE Trans. Sustain. Energy*, vol. 7, no. 3, pp. 1133–1144, Jul. 2016.

[17] K. Hua, Y. Mishra, and G. Ledwich, "Fast unscented transformation-based transient stability margin estimation incorporating uncertainty of wind generation," *IEEE Trans. Sustain. Energy*, vol. 6, no. 4, pp. 1254–1262, Oct. 2015.

[18] Y. Xu, M. Yin, Z. Y. Dong, R. Zhang, D. J. Hill, and Y. Zhang, "Robust dispatch of high wind power-penetrated power systems against transient instability," *IEEE Trans. Power Syst.*, vol. 33, no. 1, pp. 174–186, Jan. 2018.

[19] Y. Xue, T. Van Custem, and M. Ribbens-Pavella, "Extended equal area criterion justifications, generalizations, applications," *IEEE Trans. Power Syst.*, vol. 4, no. 1, pp. 44–52, Feb. 1989.

[20] Y. Chen, S. M. Mazhari, C. Y. Chung, S. O. Faried, and B. C. Pal, "Rotor angle stability prediction of power systems with high wind power penetration using a stability index vector," *IEEE Trans. Power Syst.*, vol. 35, no. 6, pp. 4632–4643, Nov. 2020.

[21] R. T. F. A. King, X. Tu, and L. A. Dessaint, "Independent component analysis for feature reduction in critical clearing time estimation," in *Proc. CCECE*, Vancouver, BC, Canada, 2016, pp. 1–5.

[22] L. Breiman, J. H. Friedman, R. A. Olshen, and C. J. Stone, *Classification and Regression Trees*. Monterey, CA, USA: Wadsworth & Brooks 1984.

[23] Y. Freund and R. E. Schapire, "A decision-theoretic generalization of on-line learning and an application to boosting," *J. Comput. Syst. Sci.*, vol. 55, no. 1, pp. 119–139, Aug. 1997.

[24] J. Zhu, H. Zou, S. Rosset, and T. Hastie, "Multi-class AdaBoost," *Statist. Interface*, vol. 2, no. 3, pp. 349–360, 2009.

[25] H. Drucker, "Improving regressors using boosting techniques," in *Proc. 14th Int. Conf. Mach. Learn.*, 1997, pp. 107–115.

[26] B. W. Silverman, *Density Estimation for Statistics and Data Analysis*, vol. 26. Boca Raton, FL, USA: CRC Press, 1986.

[27] F. Pedregosa *et al.*, "Scikit-learn: Machine learning in Python," *J. Mach. Learn. Res.*, vol. 12, pp. 2825–2830, Oct. 2011.

[28] A. K. Singh and B. C. Pal, *Report on the 68-Bus, 16-Machine, 5-Area System*, document IEEE PES Task Force on Benchmark Systems for Stability Controls, Ver. 3.3, 2013.

[29] *Dynamic Parameters of Synchronous Generators and Wind Turbines*. Accessed: Dec. 10, 2020. [Online]. Available: https://1drv.ms/b/s!AuqPIf3UarwJgt47H-tN5hI767dsMQ?e=QNVVRd

[30] *Siemens Power Technologies International*, document PSS E 34.2 Program Application Guide, vol. 2, Apr. 2017.

[31] *Wind Generation & Total Load in the BPA Balancing Authority*. Accessed: Jan. 2, 2021. [Online]. Available: https://transmission.bpa.gov/Business/Operations/Wind/

[32] *PJM Hourly Metered Load*. Accessed: Jan. 5, 2021. [Online]. Available: http://dataminer2.pjm.com/feed/hrl_load_metered

[33] *IEEE Guide for Breaker Failure Protection of Power Circuit Breakers*, IEEE Standard C37.119-2016 Jul. 2016.

[34] R. D. Zimmerman, C. E. Murillo-Sanchez, and R. J. Thomas, "MATPOWER: Steady-state operations, planning and analysis tools for power systems research and education," *IEEE Trans. Power Syst.*, vol. 26, no. 1, pp. 12–19, Feb. 2011.

YUCHUAN CHEN received the B.S. and M.S. degrees from South China University of Technology, Guangzhou, China, in 2013 and 2016, respectively. He is currently pursuing the Ph.D. degree with the University of Saskatchewan, Saskatoon, SK, Canada. From January 2019 to May 2019, he was a Visiting Research Student with Imperial College London, London, U.K. His research interest includes applications of machine learning techniques in power systems with high wind power penetration.

S. MAHDI MAZHARI (Member, IEEE) received the M.Sc. degree (Hons.) in electrical engineering from the University of Tehran, Tehran, Iran, in 2012, and the Ph.D. degree (Hons.) in electrical engineering from Amirkabir University of Technology, Tehran, in 2016. He is currently working as a System Studies Consultant with PSC North America, Vancouver, BC, Canada, and a Research Associate with the University of Saskatchewan, Saskatoon, SK, Canada. His research interests include power system transient stability, renewable energy interconnection studies, and artificial intelligence applications to power system automation.

C. Y. CHUNG (Fellow, IEEE) received the B.Eng. (Hons.) and Ph.D. degrees in electrical engineering from The Hong Kong Polytechnic University, Hong Kong, China, in 1995 and 1999, respectively.

He is currently a Professor, the NSERC/SaskPower (Senior) Industrial Research Chair in smart grid technologies, and the SaskPower Chair in power systems engineering with the Department of Electrical and Computer Engineering, University of Saskatchewan, Saskatoon, SK, Canada. His research interests include smart grid technologies, renewable energy, power system stability/control, planning and operation, and computational intelligence applications.

Prof. Chung is a Senior Editor of IEEE TRANSACTIONS ON POWER SYSTEMS, the Vice Editor-in-Chief of *Journal of Modern Power Systems and Clean Energy*, and a Subject Editor of *IET Generation, Transmission and Distribution*. He is also an IEEE PES Distinguished Lecturer and a member of IEEE PES Fellow Evaluation Committee.

SHERIF O. FARIED (Senior Member, IEEE) received the B.Sc. and M.Sc. degrees in electrical engineering from Ain Shams University, Cairo, Egypt, in 1979 and 1984, respectively, and the M.Sc. and Ph.D. degrees in electrical engineering from the University of Saskatchewan, Saskatoon, SK, Canada, in 1988 and 1993, respectively.

From 1979 to 1984, he was a Teaching and Research Assistant with the Department of Electrical Power and Machines, Ain Shams University. He is currently a Professor of electrical engineering with the Department of Electrical and Computer Engineering, University of Saskatchewan. His current research interests include power system dynamics, control, reliability, protection, and power quality.

Prof. Faried is a Registered Professional Engineer at the Province of Saskatchewan, Canada.

• • •